Supplemental Materials

Molecular Biology of the Cell

Higashi et al.

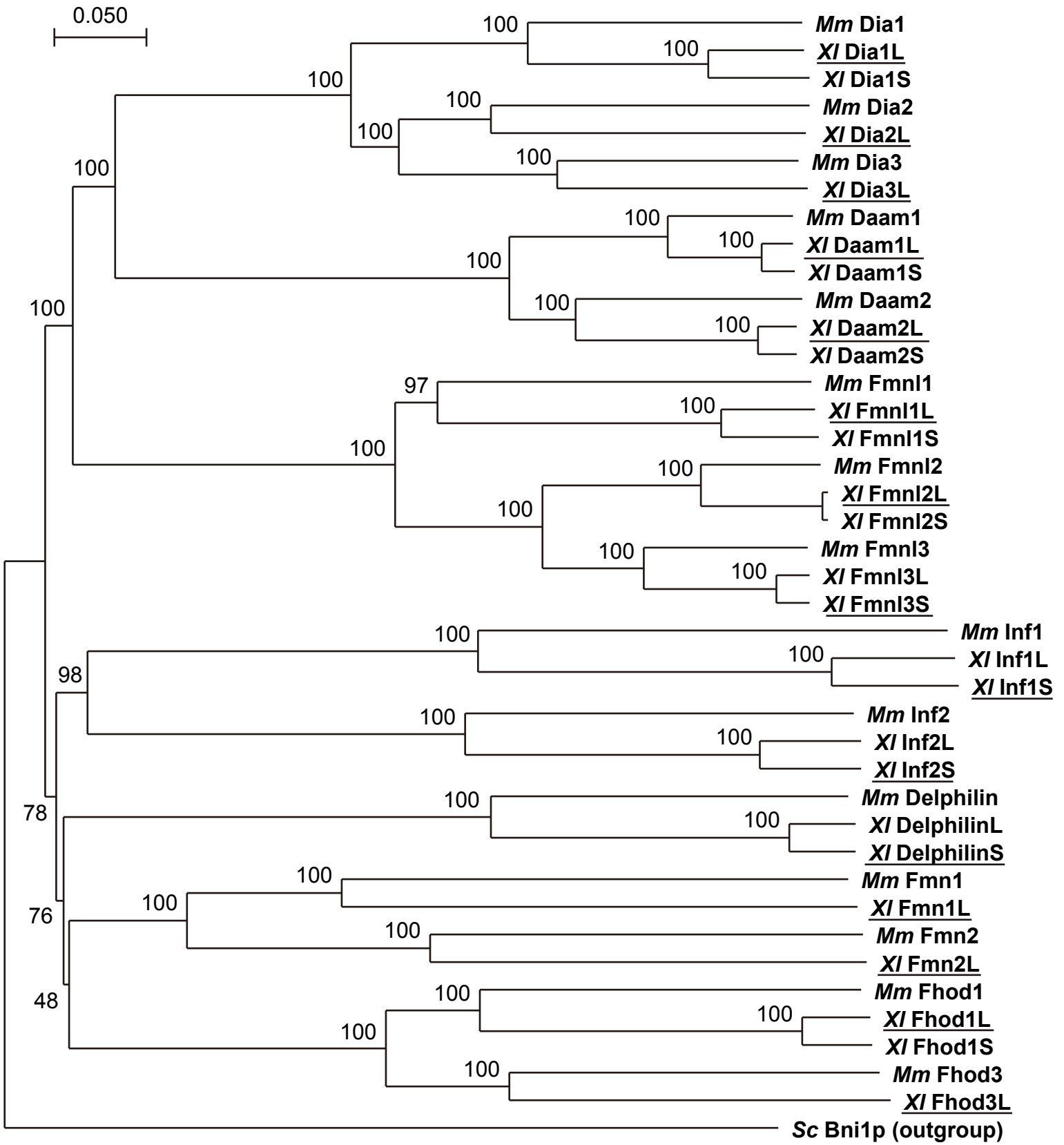

FIGURE S1: **A phylogenic tree of formins using the neighbor-joining method.** Numbers on the branches indicate the percentage of occurrences of branches in 1000 bootstrap trials. Yeast Bni1p sequence serves as an outgroup. Sequences used in this study are underlined. Since *X. laevis* is allotetraploid, both alloalelles are included and designated L and S. Since the genome sequencing of Dia2S and Dia3S locuses is not completed, these sequences are not included. Scale bar indicates the rate of amino acid substitutions per site. *Mm*, *Mus musculus*, *Xl*, *Xenopus laevis*, *Sc*, *Saccharomyces cerevisiae*.

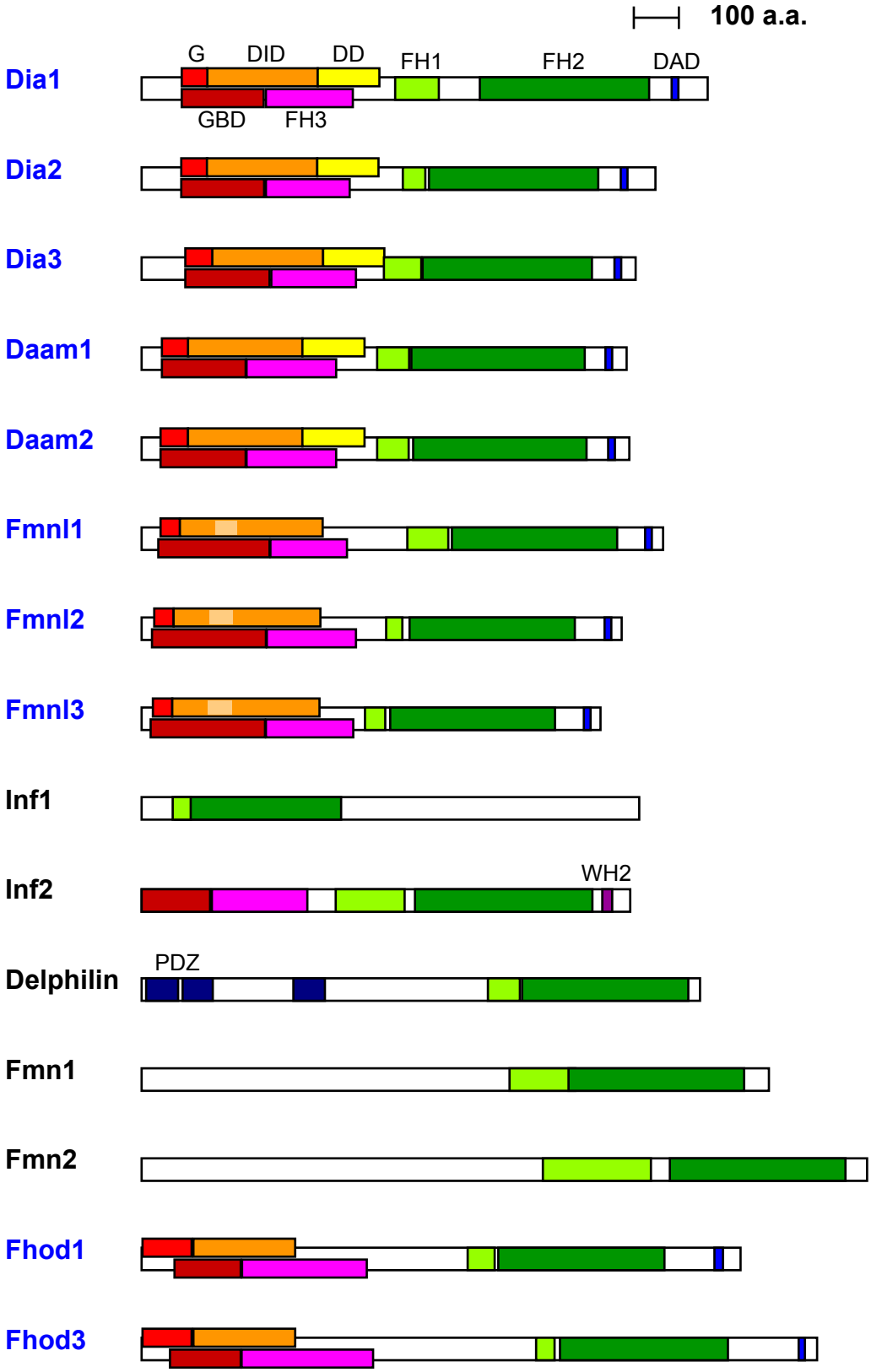

FIGURE S2: **Domain structures of 15 *Xenopus laevis* formins based on Smart and Pfam databases.** For DRFs (blue font), GBD and FH3 domains were originally proposed based on homology. Later, G, DID and DD domain organization was proposed based on crystal structure information. Both domain annotations are shown here. For Fmnl1-3, there is an insertion in the DID domain, which is depicted in light orange here. G, GTPase binding region (red); DID, diaphanous inhibitory domain (orange); DD, dimerization domain (yellow), FH1, formin homology 1 (light green); FH2, formin homology 2 (green); DAD, diaphanous autoinhibitory domain (blue); GBD, GTPase-binding domain (dark red); FH3, formin homology 3 (pink); WH2, WASP homology 2 (purple); PDZ, PSD-95/Dlg/ZO-1 domain (dark blue).

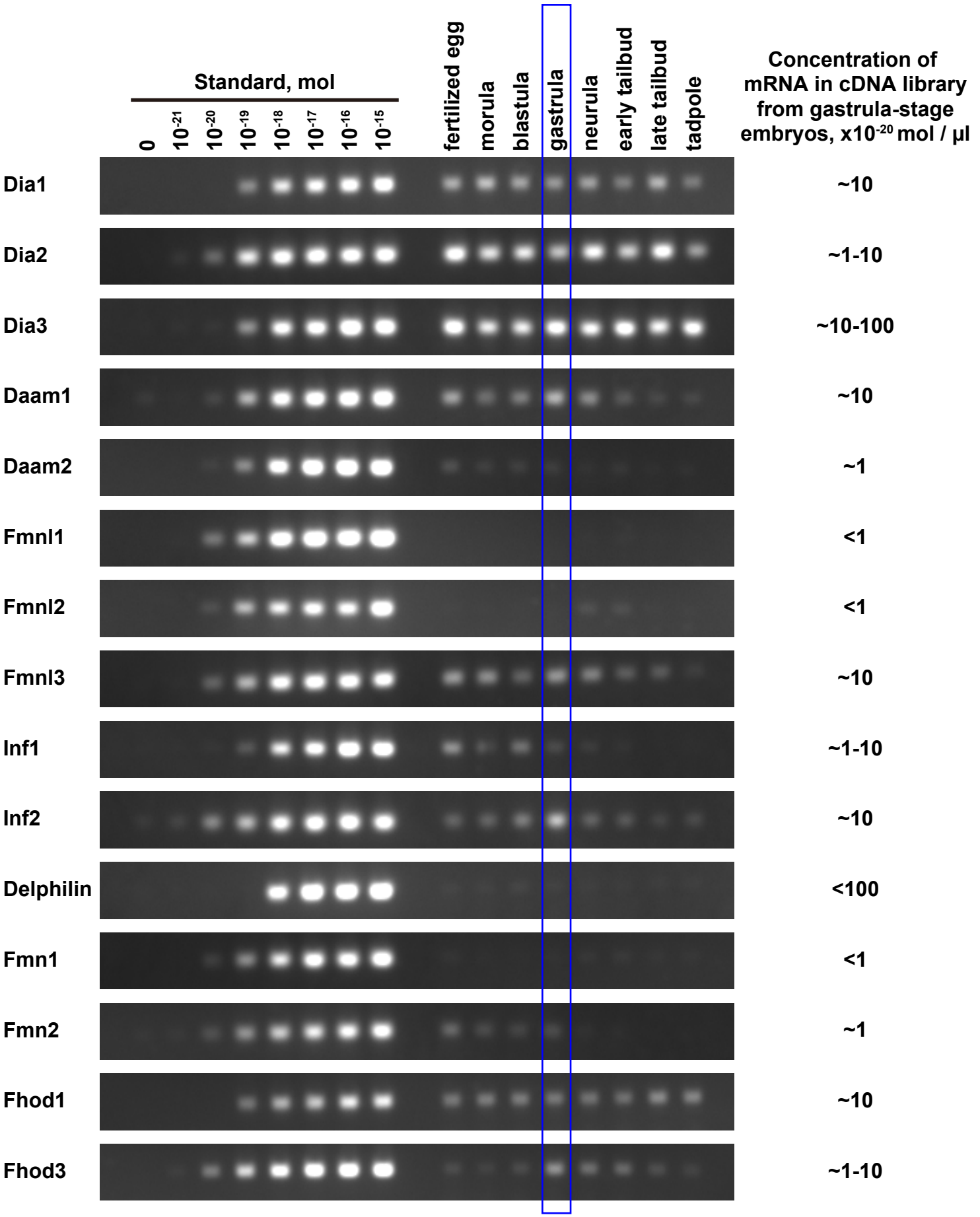

FIGURE S3: **Semi-quantitative RT-PCR of formins at various *X. laevis* developmental stages.** cDNAs from each developmental stage were examined with specific primers for each of the 15 formins. DNA fragments of each formin were amplified from late tailbud-stage, diluted sequentially, and used as standards. Concentrations of mRNAs of formins at gastrula-stage estimated by the intensity of bands is shown on the right. Note that at least 10 formins are expressed in gastrula stage.

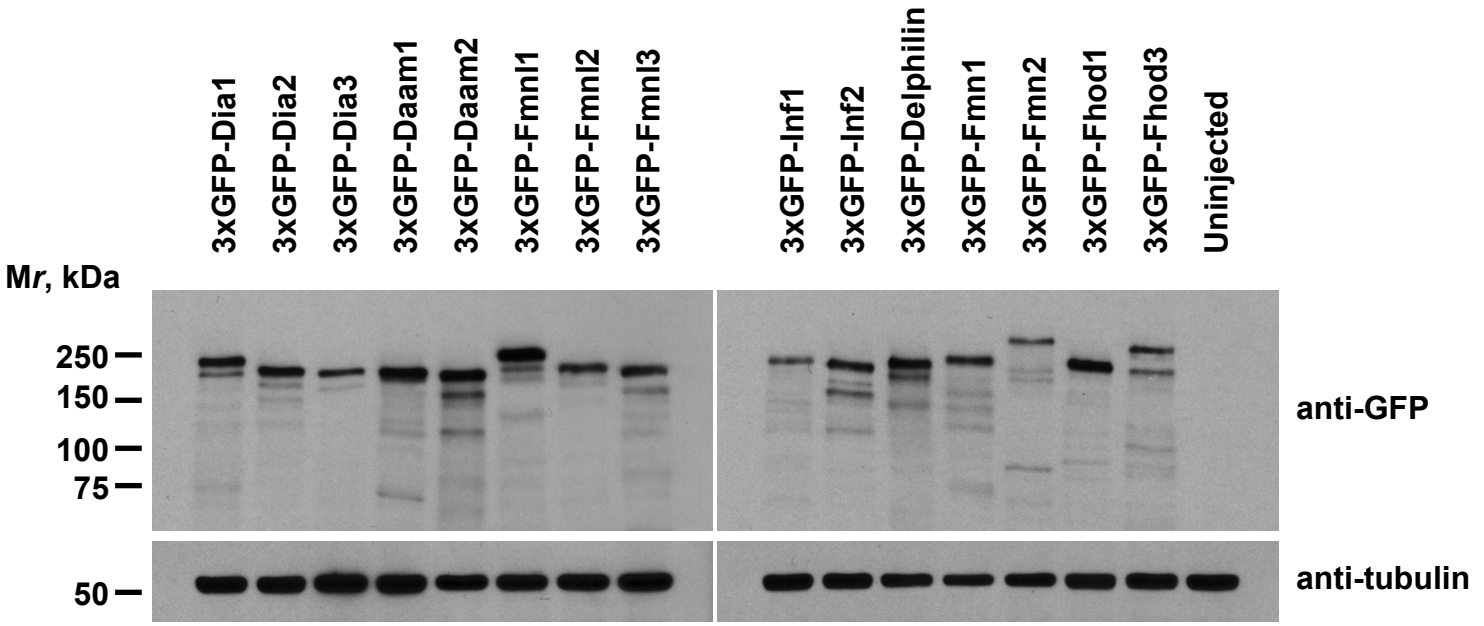

FIGURE S4: **Immunoblot analyisis of embryos expressing 3xGFP-tagged formins.** Lysates from gastrula-stage embryos expressing 3xGFP-tagged formins were subjected to immunoblotting using anti-GFP and anti-tubulin antibodies. Note that all formins are expressed and observed at near expected size.

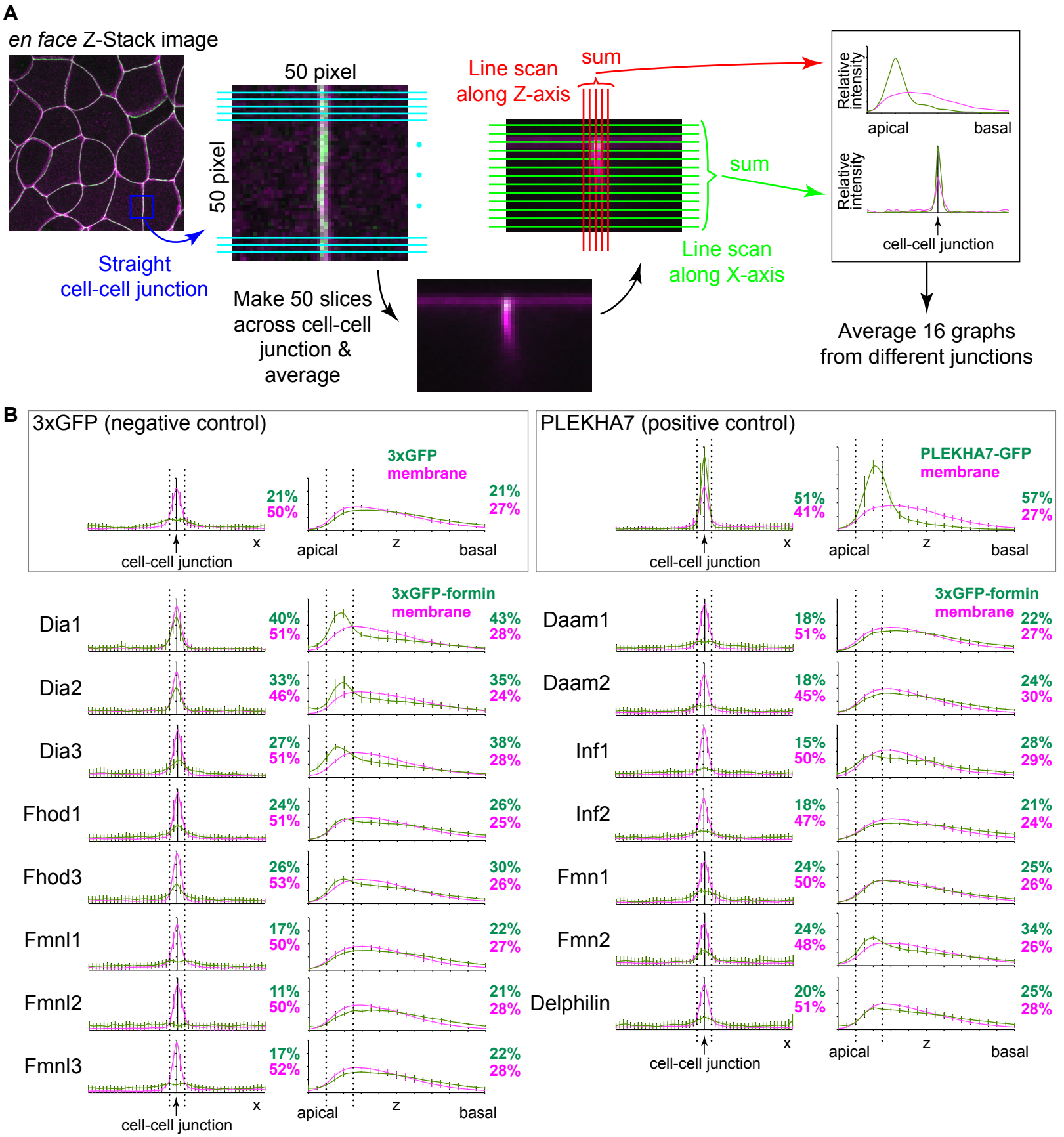

FIGURE S5: **Quantification of the localization of formins at cell-cell junctions.** A. Stacked images (50 pixel x 50 pixel) of straight junctions in 3xGFP-formin- and mCherry-farnesyl (membrane probe)-expressing embryos were taken. 50 slices across the cell-cell junction were averaged. Fluorescence intensity profiles along X-axis and Z-axis were determined by multiple line scans (n=16 from 4 different embryos) and plotted as a ratio to total fluorescence. B. Fluorescence intensity profiles of 3xGFP formin (green) and membrane probe (magenta) are shown. 3xGFP alone and PLEKHA7-GFP (AJ marker) were used as negative and positive control, respectively. Numbers next to the graphs indicate the area between dotted lines, showing the extent of junction localization. Error bars indicate s.d..

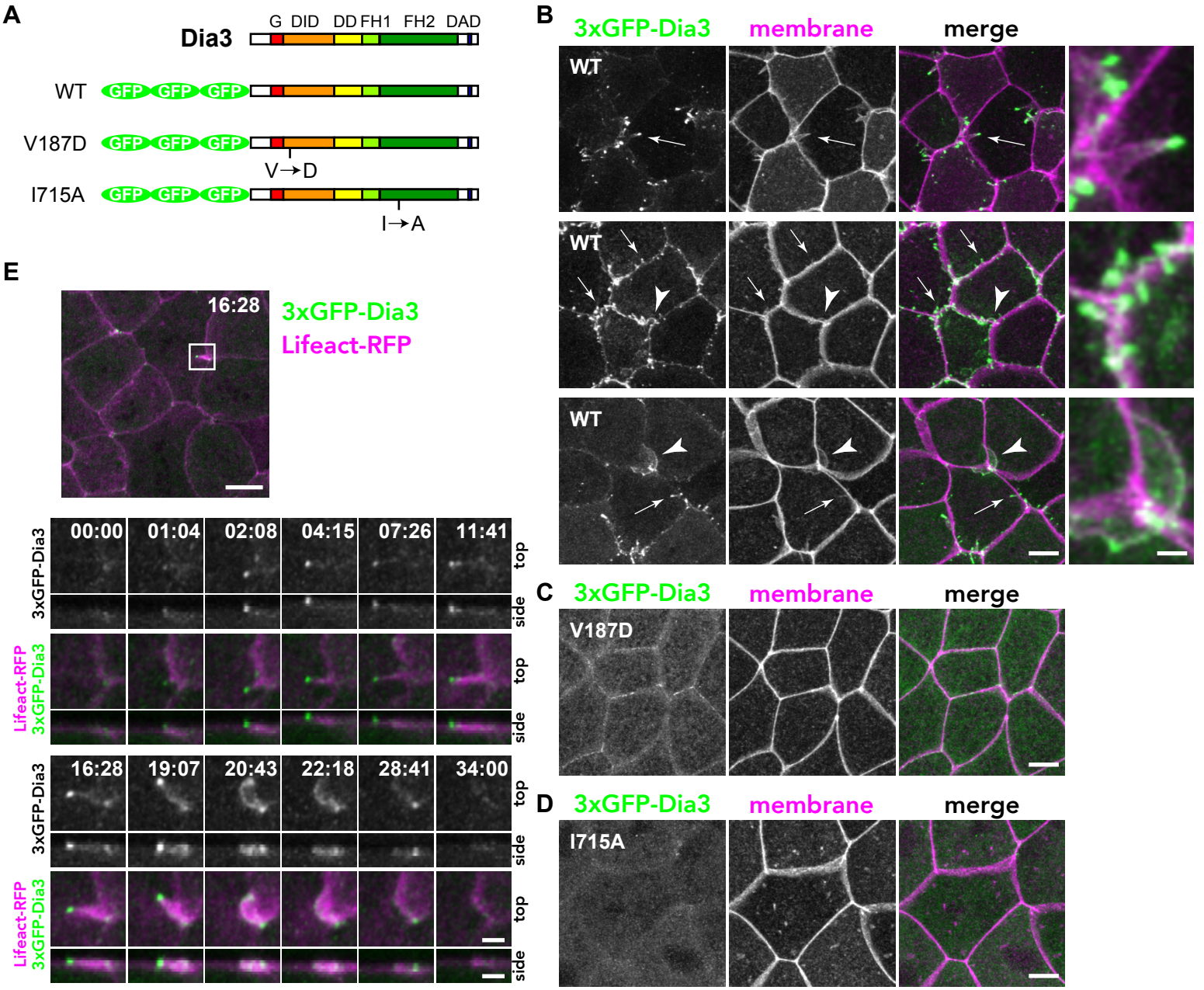

FIGURE S6: **Exogenous expression of Dia3 induces abnormal apical filopodia and lamellipodia formation at cell-cell junctions.** A. Dia3 constructs. B-E. Embryos expressing mCherry-farnesyl (membrane probe, magenta) and 3xGFP-Dia3 WT (B), V187D (C), or I715A (D) (green) or Lifeact-RFP (F-actin probe) and 3xGFP-Dia3 WT (E). Note that Dia3 WT induces filopodia-like (arrows) and lamellipodia-like (arrowheads) structures between adjacent cells while V187D and I715A do not and that Dia3 is localized at the tips of actin-rich filopodia-like protrusions and surface of lamellipodia-like structure. Scale bar, 10 μm (B left, C, D, E top image); 2 μm (B right, E bottom images).

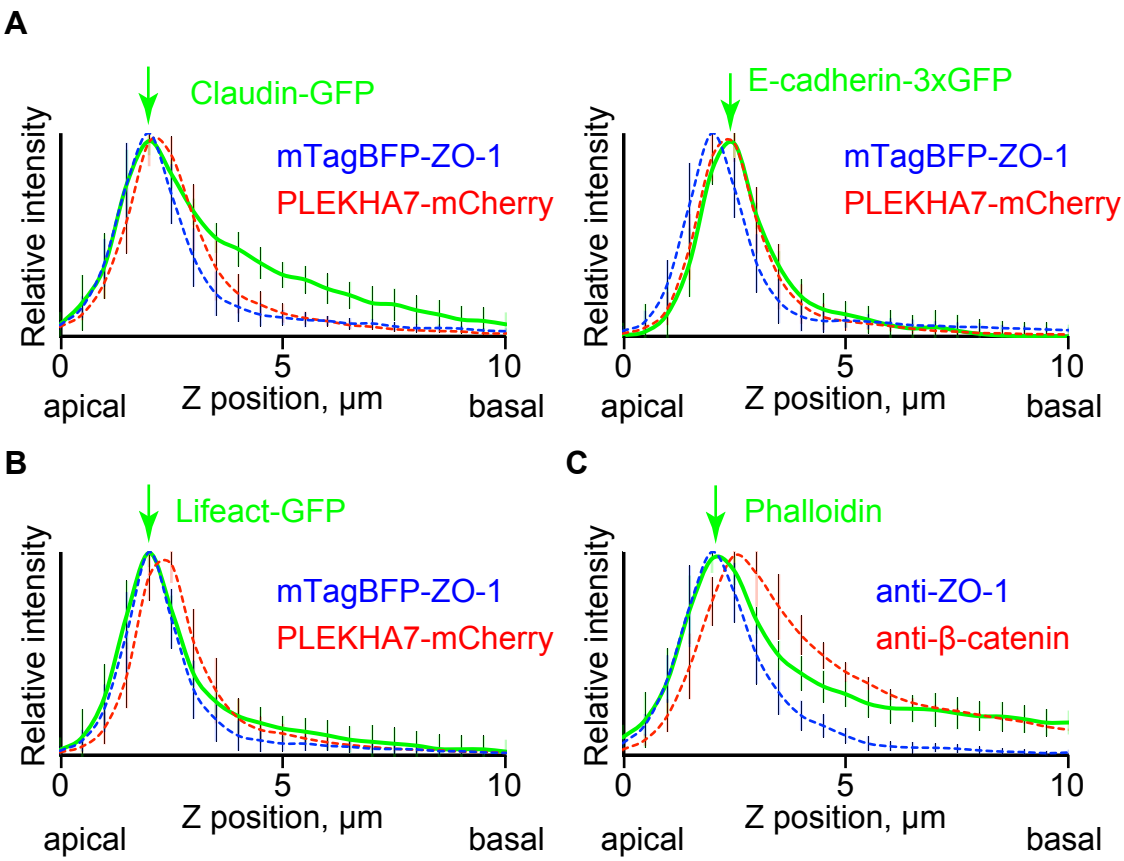

FIGURE S7: **TJ-associated F-actin bundle is evident in *X. laevis* epithelial cells.**
A. Embryos expressing Claudin (XCla)-GFP (TJ component) or E-cadherin-3xGFP (AJ component) together with mTagBFP-ZO-1 (TJ marker) and PLEKHA7-mCherry (AJ marker) were observed, and the fluorescence intensity of each probe along the Z-axis was determined. Note that the claudin and ZO-1 peaks overlap, and the E-cadherin and PLEKHA7 peaks overlap, indicating that ZO-1 and PLEKHA7 serve as good TJ and AJ markers, respectively. B. F-actin localization was determined using Lifeact-GFP. Note that Lifeact has a peak at the ZO-1 peak, suggesting that TJ-associated F-actin is more evident than AJ-associated F-actin. C. F-actin localization was assessed by phalloidin in fixed embryos. Embryos were stained for ZO-1, β-catenin, and phalloidin, and the fluorescence intensity along the Z-axis was detemined. Note that phalloidin signal also has a peak at the ZO-1 peak, suggesting that the TJ is enriched in F-actin. Error bars indicate s.d..

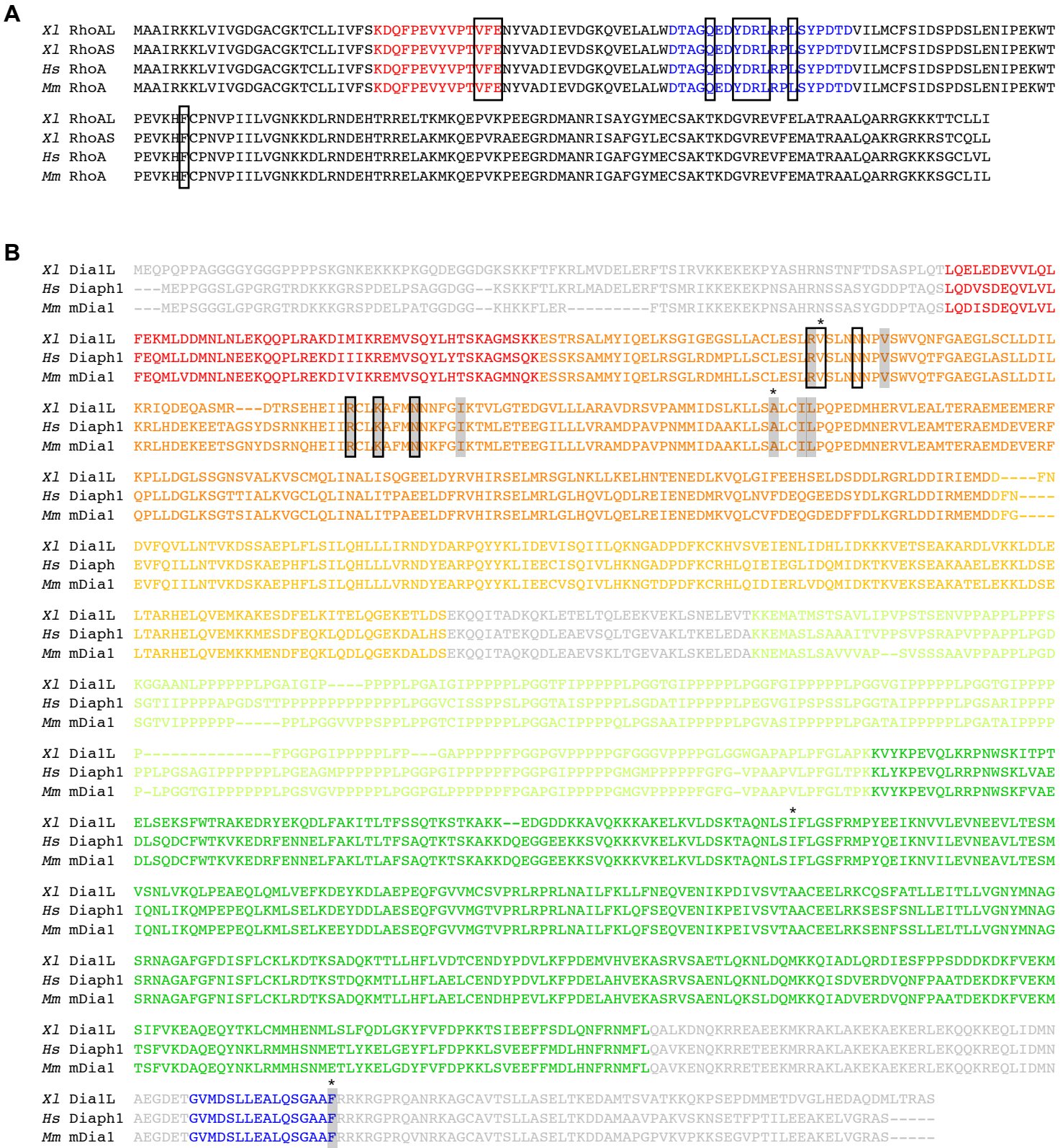

FIGURE S8: **Sequence alignments of RhoA and Dia1.** Amino acid sequences of RhoA (A) and Dia1 (B) from *X. laevis* (*Xl*), human (*Hs*) and mouse (*Mm*) were aligned. A. Switch 1 (red) and switch 2 (blue) are shown. Residues in the black boxes are important for binding to Dia1 (Rose et al., *Nature*, 2005). B. Residues important for GTP-RhoA binding (black boxes) and DID-DAD autoinhibition (gray shadow) are shown. The residues mutated in this study are shown with asterisks. Note that all mutated, boxed, and shadowed residues are conserved among *Xenopus*, human and mouse. G, red; DID, orange; DD, yellow; FH1, light green; FH2, green; DAD, blue.

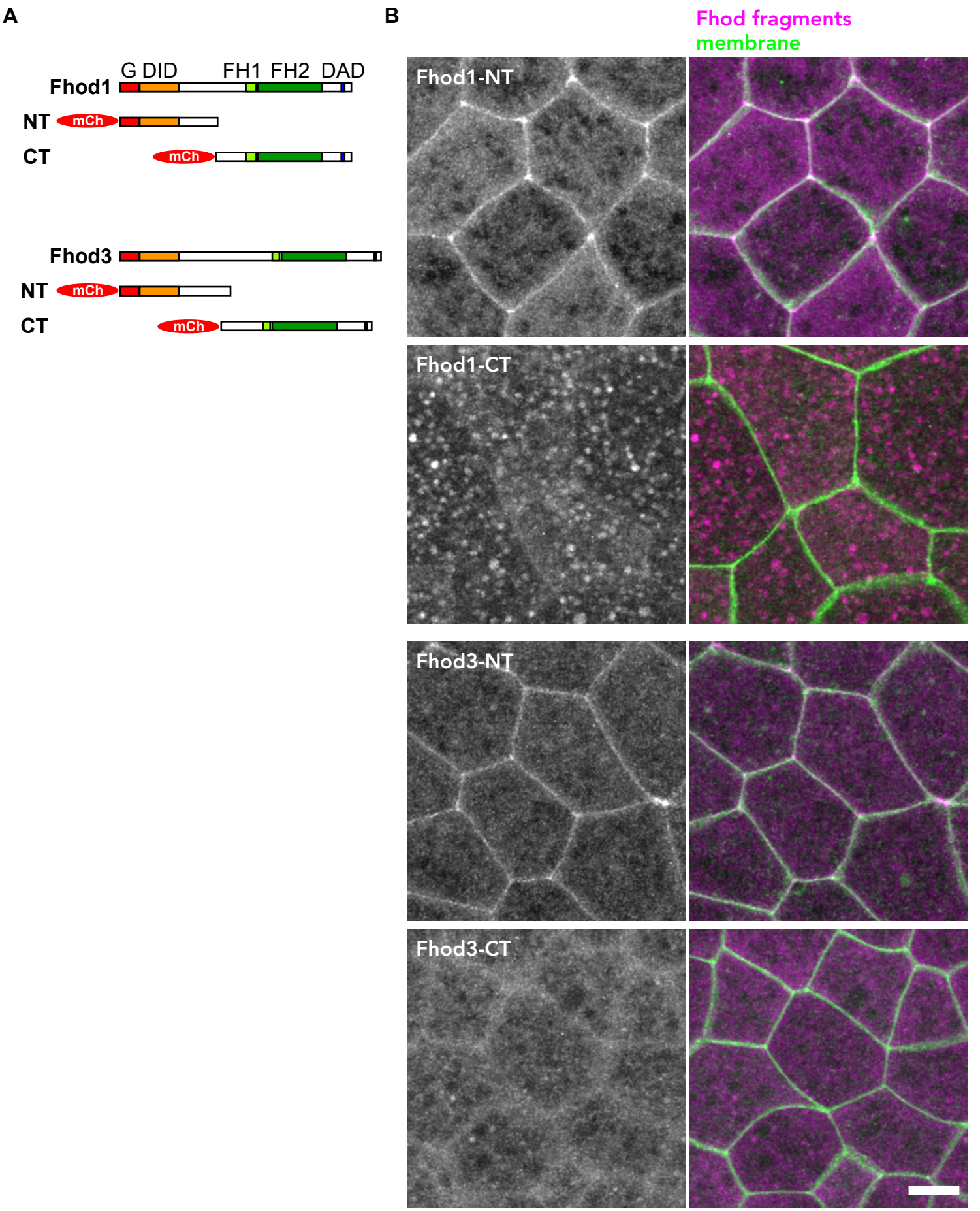

FIGURE S9: **The NT region is responsible for junctional localization of Fhod1 and Fhod3.** A. Domain structure and fragments of Fhod1 and Fhod3. B. mCherry-tagged fragments of Fhod1 and Fhod3 (magenta) were expressed with GFP-farnesyl (membrane probe; green). Note that the NT fragments are at cell-cell junctions while the CT fragments are diffusely localized in the cytoplasm. Scale bar, 10 μm.